Mechanics of Time-Dependent Materials (2023) 27:559–581
https://doi.org/10.1007/s11043-023-09606-y

RESEARCH

# High-speed impact performance of a high-performance concrete with functionally gradient structure designs

**Junlin Lv**[1] · **Zhiliang Ren**[1] · **Junhong Huang**[2]

Received: 31 March 2023 / Accepted: 23 May 2023 / Published online: 6 June 2023


**Abstract**
Ultra-high performance concrete is characterized by its high strength and high toughness, and ceramsite concrete can absorb energy and function as a buffer. Based on the mechanical properties of both, the two kinds of concrete materials are combined in the spatial structure, and three structural models, namely, gradient structure group target, double stacked structure group target, and single material structure group target, are designed and prepared. Then, the dynamic characteristics and protection performance of the three targets are compared and analyzed via experiments and numerical simulations under different projectile penetration velocities. The results show that because the two transition layers and the fiber layer between the interfaces are set in the gradient structure group target, which largely improves the resistance in the process of projectile penetration, the cratering area, cratering depth, and penetration depth of the gradient structure group target are the smallest under the same projectile penetration velocity. The larger the projectile penetration velocity is, the more outstanding the penetration resistance of the gradient structure group target is.

**Keywords** Ultra-high performance concrete · Ceramsite concrete · Gradient structure group target · Penetration speed · Penetration depth

## 1 Introduction

Concrete is widely used in the field of military protection because of its high strength. Most studies also show that the penetration resistance of concrete protective structures increases with its strength (Dancygier et al. 2007; Li et al. 2005). However, Cheng et al. (2015) believes that when the concrete grade is higher than 100 MPa, the ductility and fracture toughness of the concrete should be taken into account if the penetration resistance of the concrete is to be significantly improved. Therefore, to improve the protective performance of concrete, it is necessary to improve the toughness of concrete in addition to high strength. Pan

✉ J. Lv
JLLv_sdtbu@163.com

1 School of Management Science and Engineering, Shandong Technology and Business University, Yantai, 264005, Shandong, China

2 School of Resources and Environmental Engineering, Wuhan University of Technology, Wuhan, 430070, Hubei, China

and Ma (2017) added a certain volume of fiber to cement concrete to significantly improve its toughness of the concrete. Sovják et al. (2015) believes that adding fiber to cement-based composites can significantly improve the penetration resistance of the target. Tai (2009) binding assay and LS-DYNA numerical analysis found that, with the increase of fiber volume content, the penetration depth and crater diameter of the projectile body decrease to a certain extent. Wang et al. (2016) also used the test and LS-DYNA numerical simulation methods to study the penetration resistance of concrete under different fiber types and volume mixtures.

To further improve the protective performance of concrete single-layer structures, the theory of multilayer composite structural materials is gradually introduced. Yang (2009) pointed out that compared with the single fiber concrete protective structure, the penetration depth of the composite protective structure can be reduced by 1/3. Wang and Dong (2009) used LS-DYNA values to study the penetration resistance of composite structure targets under different initial velocity projectiles. Yang et al. (2005) pointed out that the multilayer composite structure design can significantly improve the penetration resistance of the structure. As a special composite structural material, gradient functional structural materials have more unique advantages (Huan and Wen 2010). Zhou (2014) has systematically researched the experimental preparation of explosive composite functionally gradient target, the failure mechanism under impact penetration, and the establishment of a theoretical calculation model. Quek et al. (2010) pointed out that under the action of projectile penetration with the same velocity, the pit area of the positive penetration surface of functionally graded cement board is much smaller than that of conventional mortar board. Mastali et al. (2015) believes that gradient design can significantly enhance the impact resistance of concrete slabs.

Because of the complex and changeable process of projectile body penetrating concrete target, it is affected by multiple factors. It is difficult to explain and solve the problem clearly by using only one of the methods of experiment, theoretical analysis, and numerical simulation. For example, the formula obtained by the experimental method has great limitations, and there are many assumptions in the theoretical analysis method, while the relevant parameters in the numerical simulation method are mostly from the empirical formula. Therefore, based on the comprehensive analysis of the research methods on the penetration of concrete by the projectile body, this paper adopts the method of combining experimental method and numerical simulation in the research on the penetration performance of structural materials with high impact gradient, to fully interpret and describe the dynamic response of structural materials with high impact gradient under the action of projectile body penetration. At the same time, it is expected to provide some theoretical guidance for the design and preparation of cement-based functional gradient structural materials.

## 2 Gradient functional structural materials

### 2.1 Mechanical mechanism of projectile penetration through multilayer medium

The process of projectile penetration into a concrete target can be divided into the pitting stage and the stable penetration stage. In the cratering stage, the acceleration of the projectile body appears as a rapidly rising instantaneous pulse, while in the stable penetration stage, the acceleration changes relatively gently. The resistance of the projectile body along its axis can be expressed as Gao et al. (2012):

$$F = Cz, \qquad 0 \le z \le 4a \tag{1}$$

$$F = \pi a^2 \left(R + N\rho V^2\right), \qquad 4a \le z \le P \tag{2}$$

In the formula, $F$, $z$, and $V$ are the instantaneous resistance, displacement, and velocity of the projectile body; $C$ is the undetermined coefficient; $a$ is the Body radius. $R$ is related to static resistance. If the complexity of the material is not considered, it can be directly determined by the test results. $N\rho V^2$ is related to dynamic resistance; $\rho$ is the initial density of the target; $P$ is the Ultimate penetration depth. Formula (2) is derived from cavity expansion theory.

For the oval warhead, $N = (8\psi - 1)/24\psi^2$, $\psi = r/2a$, $r$ is the radius of curvature of the bullet. Based on the above analysis and through Newton's second law and initial conditions, we can get the following:

$$P = \frac{m}{2\pi a^2 \rho N} \ln\left(1 + \frac{N\rho V_k^2}{R}\right) + 4a, \qquad P > 4a \tag{3}$$

$$A = \frac{\pi a^2}{m}\left(R + N\rho V_k^2\right), \qquad C = \frac{\pi a}{4}\left(R + N\rho V_k^2\right), \qquad V_k^2 = \frac{mV_s^2 - 4\pi a^3 \rho}{m + 4\pi a^3 N\rho} \tag{4}$$

$$R = \frac{N\rho V_s^2}{\left(1 + \frac{4\pi a^3 N\rho}{m}\right)\exp\left[\frac{2\pi a^2 (P-4a)N\rho}{m}\right] - 1} \tag{5}$$

In the formula, $A$ is the maximum body overload; $V_s$ is the initial velocity; $V_k$ is the remaining velocity of the projectile at the end of the crater-forming phase; $R$ can be determined by Equation (5) according to a series of penetration test data. Based on the experimental results, the expression of concrete medium $R$ is obtained through the test results:

$$R = Sf_c \tag{6}$$

In the formula, $S = 82.6 f_c^{-0.554}$ or $S = 72.0 f_c^{-0.5}$

For multilayer rock and soil media, if the thickness of each layer is $T_n$ ($n = 1, 2 \ldots, N$; $N \ge 2$), according to Formula (3), the penetration depth-$H_n$ is calculated when the $n$th layer is infinite thickness. If $H_n \le T_n$, the motion law of the projectile body in the $n$ layer is calculated according to the following formula:

$$a_n = \frac{-\frac{\pi a^2 S f_c'}{m}}{\cos^2\left\{\arctan\left[\left(\frac{N\rho}{Sf_c'}\right)^{1/2} V_{n-1}\right] - \frac{\pi a^2}{m}\left(Sf_c' N\rho\right)^{1/2}(t - t_{n-1})\right\}} \tag{7}$$

$$z_n = \frac{m}{\pi a^2 N\rho} \ln\left\{\frac{\cos^2\left\{\arctan\left[\left(\frac{N\rho}{Sf_c'}\right)^{1/2} V_{n-1}\right] - \frac{\pi a^2}{m}\left(Sf_c' N\rho\right)^{1/2}(t - t_{n-1})\right\}}{\cos^2\left\{\arctan\left[\left(\frac{N\rho}{Sf_c'}\right)^{1/2} V_{n-1}\right]\right\}}\right\} \tag{8}$$

$$+ T_1 + \cdots + T_{n-1}$$

If $H_n > T_n$, the residual velocity $V_n$ and the experience time $t_n$ of the projectile body through the $n$th layer can be calculated by following the formula:

$$V_n = \left(\frac{1}{N\rho}\right)^{1/2}\left[\left(Sf_c' + N\rho V_{n-1}^2\right)\exp\left(-T_n \frac{2\pi a^2 \rho N}{m}\right) - Sf_c'\right]^{1/2} \tag{9}$$

**Table 1** Comparison of mechanical properties of three concretes

| Name | Compressive strength/MPa | Flexural strength/MPa | Modulus of elasticity/GPa | Toughness index/(J/m$^2$) | Frost resistance index/(g/cm$^2$) | Fracture energy/(J/m$^2$) |
|---|---|---|---|---|---|---|
| Ordinary concrete | 20∼50 | 2∼6 | 30∼40 | 120 | >1000 | 60 |
| High-performance concrete | 60∼120 | 6∼15 | 30∼40 | 1000∼5000 | 900 | 140 |
| Ultra-high performance concrete | 150∼800 | 25∼60 | 40∼60 | 15000∼40000 | 10 | 20000∼40000 |

$$t_n = t_{n-1} + \frac{\arctan\left[\left(\frac{N\rho}{Sf_c'}\right)^{1/2} V_{n-1}\right]}{\frac{\pi a^2}{m}\left(Sf_c' N\rho\right)^{1/2}} - \frac{1}{\frac{\pi a^2}{m}\left(Sf_c' N\rho\right)^{1/2}} \arccos\left\{\cos\left[\arctan\left(\frac{N\rho}{Sf_c'}\right)^{1/2}\right] \exp\left(\frac{T_n \pi a^2 \rho}{m}\right)\right\} \tag{10}$$

The residual velocity $V_n$ at the $n$th layer and the experience time $t_n$ are calculated in the same manner as above until the body velocity is zero.

## 2.2 Gradient functional structural component material design

### 2.2.1 Ultra-high performance concrete

Ultra-high performance concrete is a cement-based composite material with ultra-high strength and high toughness prepared based on the principle of maximum packing density. Compared with ordinary concrete and high-performance concrete materials, ultra-high performance concrete protective structural materials have outstanding excellent performance. The mechanical property data of three kinds of concrete are all derived from the summary of a large number of mechanical experimental results, as shown in Table 1.

Therefore, in this paper, the ultra-high performance concrete is selected as the main anti-penetration component of the protective structure; through the ultra-high strength and toughness of ultra-high performance concrete, the opening depth, opening area, and penetration depth of the projectile body on the interface of the concrete target can be reduced to the greatest extent.

### 2.2.2 Ceramsite concrete

When the concrete target structure is subjected to the impact force of the projectile body, in addition to certain damage and destruction on the front of the concrete target structure, it will also form a certain caving area on its back due to the propagation of the impact stress wave, and the movement of the caving block splash is likely to cause greater "secondary harm" to the facilities and personnel within the structure. Therefore, the concrete target structure must have a certain energy absorption buffer effect. Compared with ceramics, rocks, and other materials with higher compactness, porous structural materials exhibit better damping performance under load. Under the action of load, the porous material exhibits an incremental hardening deformation process, and its stress-strain curve can be divided into three stages: elastic section, yield plastic section, and compaction section, as shown in Fig. 1.

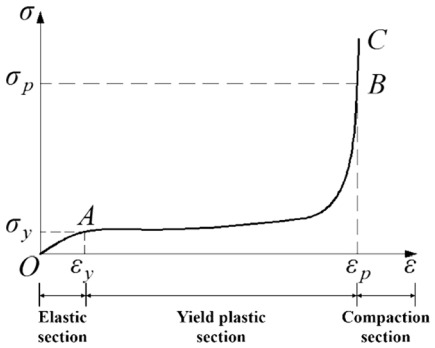


**Fig. 1** Stress-strain curve of porous material under load

As shown in Fig. 1, porous materials can undergo large deformation under load, and their stress almost remains unchanged at this stage. Porous materials can change much energy absorbed into plastic energy and dissipate heat energy in this process to play a cushioning and damping effect. Based on the unique advantages of porous structural materials in the process of energy absorption and consumption and the outstanding characteristics of ceramsite concrete as structural materials, this paper selects porous ceramsite concrete structural materials as the energy absorption buffer layer in the whole structure design process of concrete target protective structure (Kong 2008).

### 2.2.3 Functional gradient structure model

Based on the protective structure of ultra-high-performance concrete and porous ceramsite concrete, a gradient functional protective structure model is proposed, which is named ultra-high performance concrete (outer layer of structure), gradient transition layer, and porous ceramsite concrete (inner layer of structure)). In this protective structure, the outer layer of the structure is made of ultra-high performance concrete to increase the resistance of projectile penetration; in order to reduce the crater depth, crater area, and penetration depth of the projectile body, the inner layer of the structure uses ceramide concrete to absorb the shock wave of the projectile body, which has the effect of shock absorption. The intermediate gradient transition layer is composed of the outer layer and the inner layer of the structure with different content; thus, it has some major properties of both the outer and inner layers of the structure. The wave impedance matching between the outer and inner layers can be reduced to a large extent to maximize the protection performance of the whole structure.

The gradient functional protection structure model appears to be a uniform distribution of material components at the macro level, but the composition of materials varies greatly in different parts of the microstructure. Suppose the change of components of concrete structural materials in the microscopic degree also follows the law of the change of components of gradient structural materials, gradient stratification technology should be adopted in the design and preparation process of the intermediate gradient transition layer. In that case, that is, the gradient transition layer should be stratified. As shown in Fig. 2, based on the multi-phase stratification method, the layered changes of composition and content from the outer layer to the inner layer are realized. The black dots in Fig. 2 represent ultra-high performance concrete, and the white dots represent high-performance porous ceramsite concrete.

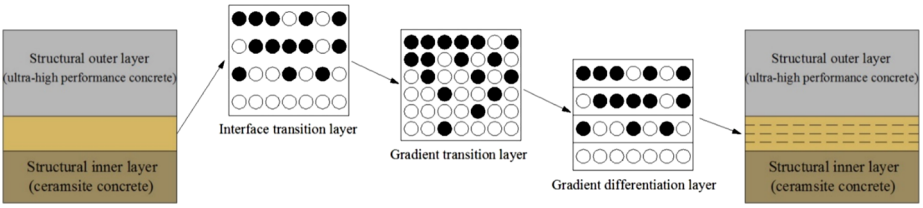


**Fig. 2** Description of functional gradient structure design and model

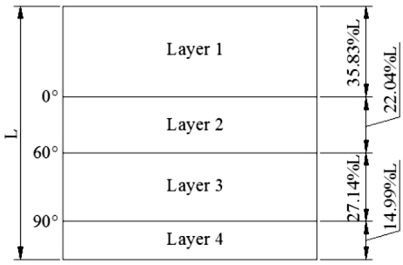


**Fig. 3** Description of gradient functional structure component

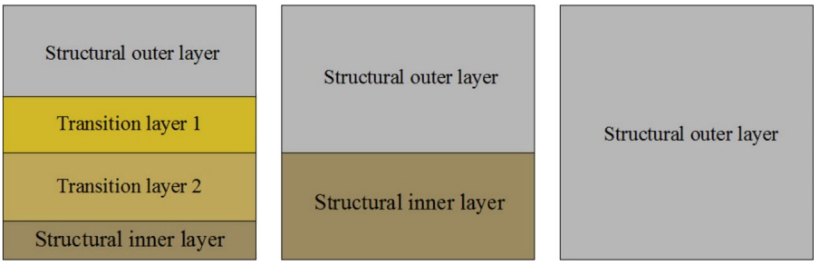


**Fig. 4** Description of structural composition distribution and structure model of the test sample

## 3 Experimental study on penetration resistance of gradient functional structural materials

### 3.1 Sample making and testing process

Referring to the design method of gradient structure optimization proposed by Wang (2013), the gradient structure with gradient distribution index b = 0.5 is optimized, and the functional gradient structure group is divided into four layers, Layer 1 (pure structural outer layer), Layer 2 (63% outer structure +37% inner structure), Layer 3 (38% outer structure +62% inner structure) and Layer 4 (pure structural inner layer), the structure diagram is shown in Fig. 3. The thickness of the outer layer of the double-laminated structure group is the sum of the thickness of the first and second layers of the gradient structure group, while the thickness of the inner layer is the sum of the thickness of the third and fourth layers. The model diagram of the functional gradient structure group, double-layered functional structure group, and single material structure group is shown in Fig. 4.

After a series of mix ratio tests and mechanical properties, the mix ratios of samples from the first layer to the fourth layer of the functional gradient structure group are determined to be A1, A2, A3, and B1, respectively. In the double-layered functional structure group, the

mix ratio of the first and second layer material is A1 and B1, respectively. The sample mix ratio of the single material structure group is A1. The specific sample coordination is shown in Table 2 and Table 3.

The model is prepared according to the structural component distribution diagram of the three test samples in Fig. 4. Due to the particularity of the artillery shooting test instrument and the special requirements of the samples, and considering the boundary effect, the upper test sample is 36.1 cm in diameter and 24 cm in thickness after theoretical calculation. The lower layer is a 16 cm thick M40 mortar cushion, and the upper and lower layers are poured in layers.

The test is conducted in the Tangshan Military Industry Test Center of Nanjing University of Science and Technology. The test process is as follows: First, the test sample (as shown in Fig. 5) is fixed by hoisting equipment and other related equipment, and then the high-speed camera (2000 frames per second), tin foil target, baffle, and firing gun are also fixed and installed, respectively. When all the equipment is installed, the projectile body obtains the initial kinetic energy to conduct a penetration test on the target through. The projectile body is made of 30CrMnSiNi2A ultra-high strength alloy steel (diameter $\times$ length: 14.5 mm $\times$ 87 mm), warhead curvature ratio CRH $= 4$, mass 65 g, hardness HRC $= 45$, and density 7850 kg/m$^3$. Its structural diagram is shown in Fig. 6. The schematic diagram of the penetration process of the whole projectile body on the target is shown in Fig. 7, and the field test process is shown in Fig. 8. After the test is completed, the pit depth, pit area, and penetration depth of samples from different test groups are recorded.

### 3.2 Test results and analysis

In the test study of the penetration performance of three kinds of targets, different initial penetration velocity is obtained by adjusting the dosage of gunpowder. The target must be pre-treated before recording the test results, including external steel pipe cutting and target profile, as shown in Fig. 9(a). The experimental measurement method is to use a vernier caliper to measure the crater diameter of the projectile body, use the rod to invade the adit of the projectile body, obtain the location of the warhead, and measure the penetration depth of the target through the rod intrusion depth. Due to the particularity of the structural form of the target, it is difficult to obtain the target, including the full penetration depth of the projectile, during the measurement of the penetration depth of the projectile. Therefore, the penetration depth of the target can be obtained only by measuring the vertical distance between the position of the warhead and the direct penetration surface of the target, as shown in Figs. 9(b) and 9(c). The impact damage of different structures can be represented by the photos of the surface of experimental samples taken after the impact test, as shown in Fig. 10.

The pitting area, pitting depth, and penetration depth of three kinds of targets under different projectile velocities are fitted and solved. The results are shown in Figs. 11–13.

As can be seen from Fig. 11, as the penetration velocity of the projectile increases, the impact force generated at the contact point between the projectile and the target also increases, and then the radial cracks generated near the impact point due to compression and shear failure will continue to increase. Therefore, the crater area increases with the projectile penetration velocity for the three structural groups of targets. Under the same penetration velocity, the gradient structure group has the smallest crater area, followed by the single material structure group, and the double-laminated structure group has the largest crater area, but there is little difference in the size of the crater area. This is mainly because the target material in contact with the projectile body is composed of the same component of ultra-high performance concrete. Under the impact of the projectile body, the dynamic response characteristics of the material are similar, so they have similar pit areas.

**Table 2** Mixing ratio of ultra-high performance concrete and ceramsite concrete and related mechanical parameters

| Number | Cement | SF | FA | Sand | | Ceramide | Quartz sand | Water | SBT | SP | Modulus of elasticity/E(GPa) | Shear modulus/G(GPa) | Compressive strength/MPa | Flexural strength/MPa |
|---|---|---|---|---|---|---|---|---|---|---|---|---|---|---|
| | | | | 0-0.6 mm | 0.6-1.25 mm | | | | | | | | | |
| A1 | 0.27 | 0.05 | 0.07 | 0.28 | 0.24 | 0 | 0 | 0.07 | 0.01 | 0 | 59.88 | 24.77 | 151.9 | – |
| A2 | 0.30 | 0.04 | 0.07 | 0.21 | 0.06 | 0.11 | 0.11 | 0.05 | 0.01 | 0.03 | 54.77 | 22.99 | 144.9 | – |
| A3 | 0.29 | 0.02 | 0.05 | 0.13 | 0.04 | 0.19 | 0.19 | 0.03 | 0.01 | 0.05 | 51.03 | 21.70 | 106.3 | 29.8 |

Note: "-" in the table indicates that the value exceeds the effective range of the test equipment

**Table 3** Mixing ratio of ceramsite concrete and related mechanical parameters

| Number | Cement | Fly ash | Ceramsite | Quartz sand | Water | SP | Modulus of elasticity/E(GPa) | Shear modulus/G(GPa) | Compressive strength/MPa | Flexural strength/MPa |
|---|---|---|---|---|---|---|---|---|---|---|
| B1 | 0.9 | 0.1 | 1.08 | 1.08 | 0.30 | 0.015 | 44.74 | 19.58 | 65.4 | 11.9 |

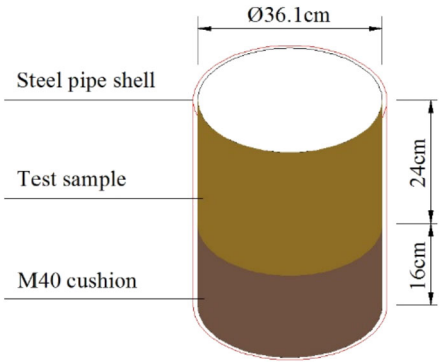


**Fig. 5** Description of test sample

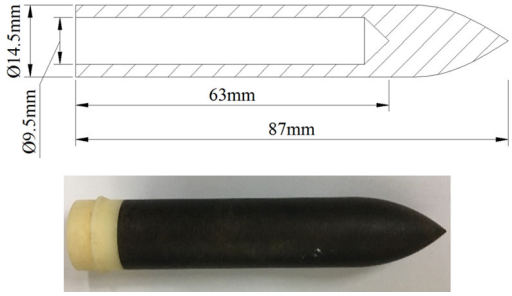


**Fig. 6** Description of bullet structure and physical objects

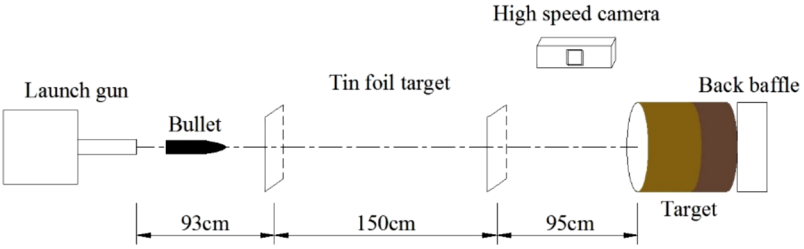


**Fig. 7** Description of the penetration test process

As can be seen from Fig. 12, with the increase of projectile penetration velocity, its crater depth will also increase. The pit depth of the double-layer structure is basically the same as that of the single-layer structure under the impact of the high-speed bullet. At the same time, through the curve fitting study of the test results of the crater depth of the target under different projectile penetration velocities, the crater depth of the target in the gradient structure group is the minimum, the crater depth of the target in the single structural material group is the second, and the crater depth of the target in the double-laminated structure group is the maximum. This may be because the structural forms of the three targets are quite different, resulting in different dynamic response characteristics of the target material in the process of the projectile body forming the funnel-shaped pit and the different penetration resistance of the projectile body in the process of penetration.

As can be seen from Fig. 13, with the increase in projectile penetration velocity, the penetration depth of the projectile body also increases. And under the impact of low-velocity bullet, the penetration depth of double-layer structure and single-layer structure is basically

**Fig. 8** Diagram of the test process

（a）**Diagram of target cutting process**

（b）**Diagram of penetration area measurement process**

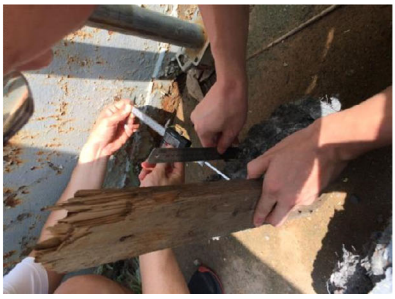

（c）**Diagram of penetration depth measurement process**

**Fig. 9** Diagram of the experimental measurement process

the same. When there is little difference in projectile penetration velocity, the penetration depth of the target in the gradient structure group is the minimum, followed by that in the single material structure group, and that in the double-laminated structure group is the maximum. At the same time, the penetration depth test results under different projectile penetration velocities are fitted. Under the same projectile penetration velocities, the penetration depth of the target in the gradient structure group is the minimum, followed by that of the target in the single material structure group, and that of the target in the Triassic structure group is the maximum, indicating that relative to the target in the single material structure group and the target in the double-laminated structure group, the penetration depth of the target in the triple structure group is the maximum. The target with a gradient structure has higher penetration resistance.

（a）Functional gradient structure group

（b）Double laminated structure group

**Fig. 10** Damage morphological diagram of the target under projectile penetration

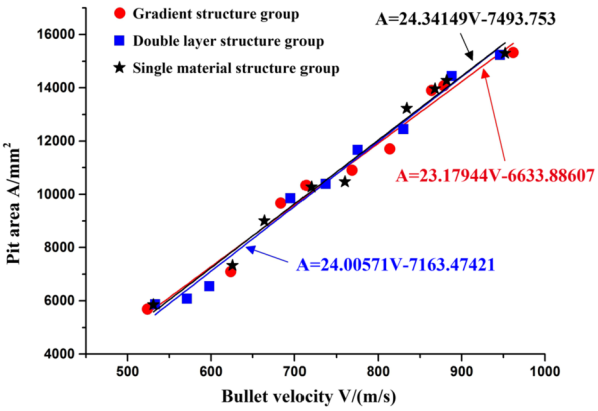


**Fig. 11** Relationship between pit area and bullet velocity

## 4 Numerical simulation of penetration resistance of functionally graded structural materials

Due to the relatively high cost of penetration tests, the number of test samples is limited, so the test results have certain limitations (Wei et al. 2022). At the same time, the stress, strain, velocity, acceleration, and other physical quantities of the projectile target system cannot be accurately measured and analyzed by penetration test. Therefore, based on the experimental results, ANSYS/LS-DYNA software is used to study the penetration resistance performance of three kinds of targets under different penetration velocities.

### 4.1 Establishment of numerical model

According to the structural symmetry of the test sample, a quarter of the three-dimensional axisymmetric finite element model is established. The thickness of the models is all 22 cm,

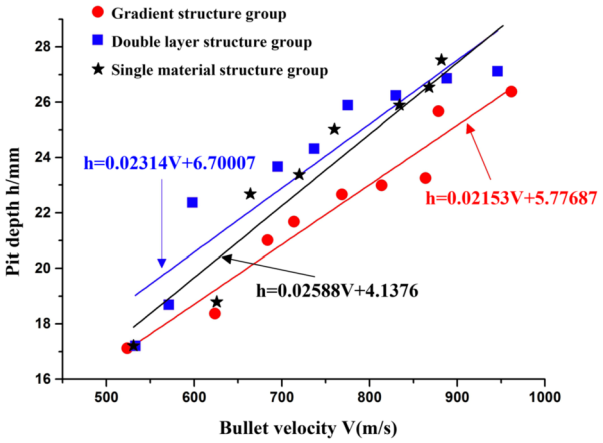


**Fig. 12** Relationship between pit depth and bullet velocity

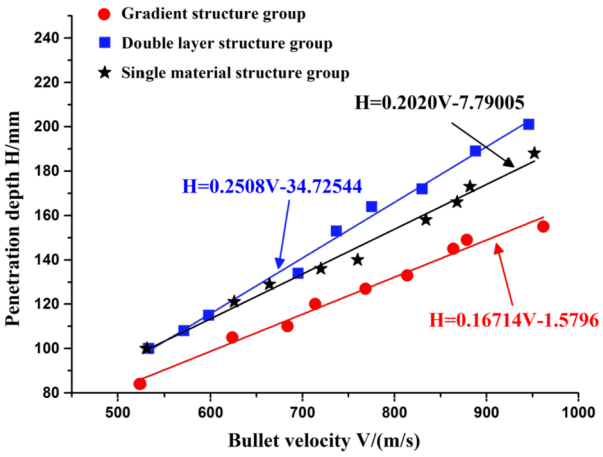


**Fig. 13** Relationship between penetration depth and bullet velocity

and the gradient structure group is 7.9 cm, 4.9 cm, 6.0 cm, and 3.2 cm from the outer layer to the inner layer, respectively. The double-laminated structure groups from the outer layer to the inner layer are 12.8 cm and 9.2 cm, respectively. The HJC model is used for all three target materials, and the total number of units is 367500. Among them, the number of units from layer 1 to layer 4 of the gradient structure group is 132,500, 82,500, 100000, and 52,500, respectively, while the number of units from layer 1 and layer 2 of the double-layered structure group is 212,500 and 155,000, respectively. Three groups of test samples are divided into SOLID 164 three-dimensional solid units, and the Lagrange algorithm is used to calculate the relevant models. In order to ensure the smooth progress of the simulation process and more accurate calculation results of the penetration problem, the contact part between the Projectile body and the target, that is, the center of the target, is divided into a relatively dense grid within 5 cm. The model diagram is shown in Fig. 14. The four color modules in the model correspond from top to bottom to A1, A2, A3, and B1 in Table 2 and Table 3.

(1) Projectile material model and parameters

Due to the particularity of the structure and size of the Projectile body, the Johnson-Cook model is adopted to divide the Projectile body into hexahedral elements, and the number of

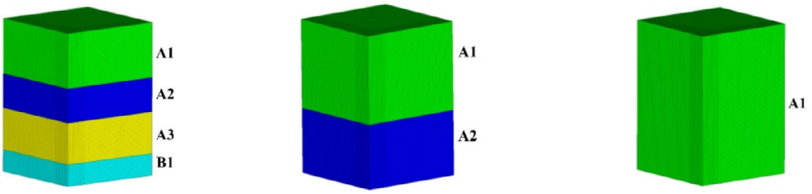


(a) Gradient structure target (b) Double layer structure target (c) Single material structure target

**Fig. 14** Description of the target model

**Table 4** Material parameters of the Projectile body (unit: cm-μs-g)

| Symbol | Meaning | Numerical value |
|---|---|---|
| $\rho$ | Density | 7.85 |
| $A$ (MPa) | Yield strength | 1280 |
| $B$ (MPa) | Hardening parameters | 800 |
| $C$ | Strain-rate sensitivity coefficient | 0.05 |
| $n$ | Strain hardening index | 0.46 |
| $m$ | Temperature softening coefficient | 1 |

**Fig. 15** Description of the bullet model

units is 3420. The related mechanical parameters of the Projectile body model are shown in Table 4. The schematic diagram of the model is shown in Fig. 15.

(2) Target material model and parameters

In numerical simulation calculation, the HJC model is adopted for target materials, and the mechanical parameters of three different structures are shown in Table 5.

(3) Boundary conditions and contact conditions

The symmetric boundary constraint is applied to the symmetric plane of the projectile body and target, and the fixed constraint is applied to the surrounding boundary of the target plate. That is, z-direction symmetric constraints are applied to the XOY plane, x-direction symmetric constraints are applied to the YOZ plane, and then non-reflective boundary conditions are applied to the x = 15 cm and z = 15 cm planes. In addition, the contact between the projectile body and the concrete target adopts an automatic surface-to-surface contact model. The initial velocity of the bullet is achieved by assigning the initial velocity to all nodes in the projectile body.

(4) Fiber layer treatment and mechanical parameters

As there are few fibers distributed between the interface of two adjacent layers of materials and their diameter is very small, it is treated as a shell in the numerical simulation calculation; the interface element with composite material properties is endowed and uses

**Table 5** Mechanical parameters of material models of different structural groups (unit: cm-μs-g)

| Symbol | Meaning | Functional gradient structure group | | | | Double-layer structure | | Single-layer structure |
|---|---|---|---|---|---|---|---|---|
| | | First layer | Second layer | Third layer | Fourth layer | Outer layer | Inner layer | |
| $\rho$ (g/cm$^3$) | Material density | 2.54 | 2.50 | 2.46 | 2.20 | 2.56 | 2.20 | 2.56 |
| $G$ (GPa) | Shear modulus | 24.14 | 23.57 | 20.19 | 18.64 | 24.14 | 18.64 | 24.14 |
| $A$/A (GPa) | Normalized cohesion strength | 0.79 | 0.79 | 0.79 | 0.79 | 0.79 | 0.79 | 0.79 |
| $B$/B (GPa) | Normalized stress hardening coefficient | 1.6 | 1.6 | 1.6 | 1.6 | 1.6 | 1.6 | 1.6 |
| $C$ | Strain-rate coefficient | 0.007 | 0.007 | 0.007 | 0.007 | 0.007 | 0.007 | 0.007 |
| $n$ | Stress hardening coefficient | 0.61 | 0.61 | 0.61 | 0.61 | 0.61 | 0.61 | 0.61 |
| $f_c$ (MPa) | Quasi-static uniaxial compressive strength | 151.9 | 144.9 | 106.3 | 90.6 | 151.9 | 90.6 | 151.9 |
| $T$ (MPa) | Maximum tensile hydrostatic pressure | 7.641 | 7.463 | 6.392 | 5.901 | 7.641 | 5.901 | 7.641 |
| $\varepsilon_{fmin}$ | Minimum plastic strain before fracture | 0.01 | 0.01 | 0.01 | 0.01 | 0.01 | 0.01 | 0.01 |
| $S_{max}$ | Normalized maximum strength | 7.0 | 7.0 | 7.0 | 7.0 | 7.0 | 7.0 | 7.0 |
| $P_{crush}$ (MPa) | Crushing pressure | 50.63 | 48.30 | 35.43 | 30.20 | 50.63 | 30.20 | 50.63 |
| $\mu_{crush}$ | Crushing volume strain | 0.0005 | 0.0005 | 0.0004 | 0.0004 | 0.0005 | 0.0004 | 0.0005 |
| $P_{lock}$ | Compaction pressure | 0.008 | 0.008 | 0.008 | 0.008 | 0.008 | 0.008 | 0.008 |
| $\mu_{lock}$ | Compaction volume strain | 0.0469 | 0.0850 | 0.1404 | 0.2182 | 0.0469 | 0.2182 | 0.0469 |
| $D_1$ | Damage constant | 0.0461 | 0.0458 | 0.0441 | 0.0431 | 0.0461 | 0.0431 | 0.0461 |
| $D_2$ | Damage constant | 1.0 | 1.0 | 1.0 | 1.0 | 1.0 | 1.0 | 1.0 |
| $K_1$ (GPa) | Pressure constant | 0.85 | 0.85 | 0.85 | 0.85 | 0.85 | 0.85 | 0.85 |
| $K_2$ (GPa) | Pressure constant | −1.71 | −1.71 | −1.71 | −1.71 | −1.71 | −1.71 | −1.71 |
| $K_3$ (GPa) | Pressure constant | 2.08 | 2.08 | 2.08 | 2.08 | 2.08 | 2.08 | 2.08 |
| $E_{pso}$ | Equivalent plastic strain | 1.0E−06 | 1.0E−06 | 1.0E−06 | 1.0E−06 | 1.0E−06 | 1.0E−06 | 1.0E−06 |

**Table 6** Mechanical parameters of fiber layer material model at the interface

| Symbol | Meaning | Numerical value |
|---|---|---|
| $\rho$ g/cm$^3$ | Density | 1.48 |
| $E_a$/GPa | Longitudinal (fiber direction) Young's modulus | 137 |
| $E_b$/GPa | Transverse (perpendicular to the fiber direction) Young's modulus | 9.4 |
| $G_{ab}$/GPa | In-plane shear modulus | 5.3 |
| $G_{bc}$/GPa | In-plane shear modulus | 3.6 |
| $G_{ca}$/GPa | In-plane shear modulus | 5.3 |
| $P_{rab}$ | Sub-Poisson ratio | 0.2 |
| $X_t$/MPa | Longitudinal (fiber direction) tensile strength | 1747 |
| $X_c$/MPa | Longitudinal (fiber direction) compressive strength | 1357 |
| $Y_t$/MPa | Transverse (perpendicular to the fiber direction) tensile strength | 80 |
| $Y_c$/MPa | Transverse (perpendicular to the fiber direction) compressive strength | 170 |
| $S_c$/MPa | In-plane shear strength | 124 |
| DFAILT | Maximum tensile strain of fiber | 0.02 |
| DFAILC | Maximum compressive strain of fiber | −0.008 |
| DFAILM | The maximum strain of the matrix in tensile and compressive modes | 0.013 |
| DFAILS | Maximum shear strain | 0.03 |
| BETA | Weight coefficient of the shear term | 0.5 |
| FBRT | The weakening coefficient of tensile strength in the fiber direction | 1.0 |
| YCFAC | The weakening coefficient of compressive strength in fiber direction after matrix compression failure | 3.0 |
| FAIL | The ratio of the current time increment to the initial time increment | 0.4 |
| SOFT | The weakening coefficient of the material strength of crushing front-end unit | 0.10 |
| EFS | Effective failure strain | 0.95 |

the material model "MAT_ENHANCED_COMPOSITE_DAMAGE" to calculate its thickness of 2 mm. The mechanical parameters of the fiber layer are shown in Table 6.

In order to better fit the penetration effect of the target in actual use, in the numerical simulation calculation, the velocity of the projectile body is set as V1 = 500 m/s, V2 = 710 m/s, V3 = 950 m/s, and its velocity value is realized by assigning initial velocity to all nodes on the projectile body model. Based on Fig. 14 and Fig. 15, numerical simulation is carried out to explore the variation rule of penetration depth and penetration resistance of the projectile body with penetration time and the failure characteristics of the target.

### 4.2 Study on penetration depth of projectile body under different structural material targets

As can be seen from Fig. 16, when the penetration velocity of the projectile body is 500 m/s, the kinetic energy of the projectile body is small, and the penetration depth of the target of the three structural groups is small different from each other. Compared with the target of the double-laminated structure group and the target of the single material structure group, the penetration depth of the target of the gradient structure group is reduced by 3.7% and 2.5%, respectively. Although the first layer of the gradient structure group, the first layer of the double-laminated structure group, and the first layer of the single material structure group

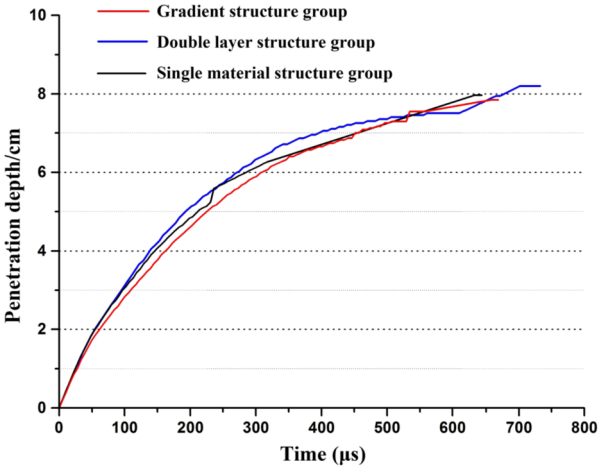


**Fig. 16** Bullet penetration depth (500 m/s)

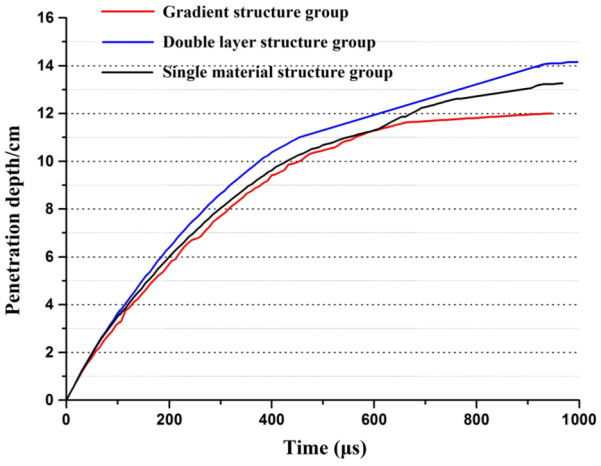


**Fig. 17** Bullet penetration depth (710 m/s)

are composed of ultra-high performance concrete, when the projectile penetrates the first layer of the gradient structure group (the outer layer of structure) and enters the second layer (transition layer 1) through the fiber interface layer, it is not only affected by the penetration resistance from the outer layer of the structure. At the same time, it will also be intercepted by the fiber layer at the interface. Hence, the penetration resistance of the projectile body is larger than that of the target of the double-laminated structure group and the target of the single-material structure group, and the final penetration depth of the projectile body is relatively small. However, the projectile body with an initial velocity of 500 m/s has been moving in the outer layer of the double-laminated structure target, so the trajectory of the projectile body in the double-laminated structure target should be the same as that of the single material structure target, that is, they have a similar penetration depth of the projectile body.

As can be seen from Fig. 17, when the projectile penetration velocity is 710 m/s, the penetration depth of the target in the gradient structure group is reduced by 16.8% and 9.9%, respectively, compared with the target in the double-laminated structure group and the tar-

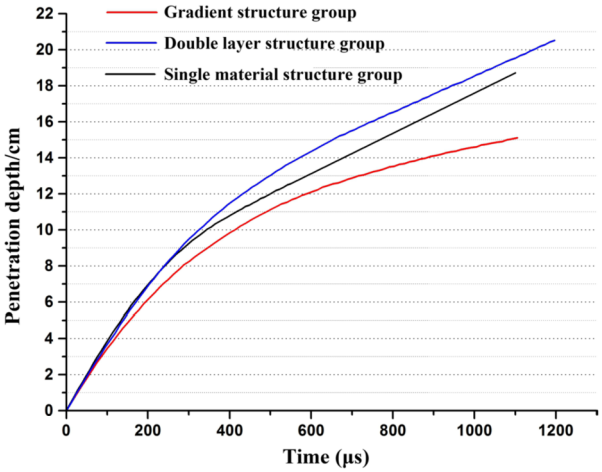


**Fig. 18** Bullet penetration depth (950 m/s)

get in the single material structure group. The penetration depth of the target in the gradient structure group is 11.9 cm; that is, the projectile body has not penetrated the second structural layer. Similarly, the projectile body has penetrated the first structural layer of the target in the double-layered structure group into the second structural layer. Compared with the first structure layer and the second structure layer of the double-laminated structure group, the target of the gradient structure group not only has the same first structure layer but also has the second structure layer (gradient transition layer) with higher toughness and strength and the fiber layer at the interface. The projectile body has to go through two kinds of materials and one interface in the process of movement, and its penetration resistance is relatively large. Hence, the gradient structure group target has a small penetration depth. The penetration depth of the single material structure group is smaller than that of the double-laminated structure group, but it is still greater than that of the gradient structure group because the structure of the single material structure group is composed of ultra-high performance concrete.

As can be seen from Fig. 18, when the projectile penetration velocity is 950 m/s, the penetration depth gap between the target of the gradient structure group and that of the target of the double-laminated structure group and the target of the single material structure group is increasingly larger, decreasing by 25.6% and 19.7%, respectively. Because the projectile body has relatively high kinetic energy, the projectile body penetrates the target of the gradient structure group through the outer layer of the structure, a fiber interface layer, a second structure layer, a fiber interface layer, and a third structure layer. For the target with a double-layered structure, the projectile penetrates through the first structural layer, the interface layer, and the second structural layer. Although ceramsite concrete has excellent energy absorption and buffering effect, its strength and toughness are lower than the second and third structural layers of the gradient structure group target. Therefore, compared with the target of the double-layered structure group, the penetration resistance of the projectile body during the process of penetrating the target of the gradient structure group is larger. At the same time, the fiber orientations at the two interfaces of the gradient structure group formed a similar network structure in the three-dimensional space Angle of the projectile body penetration, which could further improve the penetration resistance of the projectile body during the process of penetration. Therefore, the penetration depth of the target in the gradient structure group is much smaller than that in the double-laminated structure group.

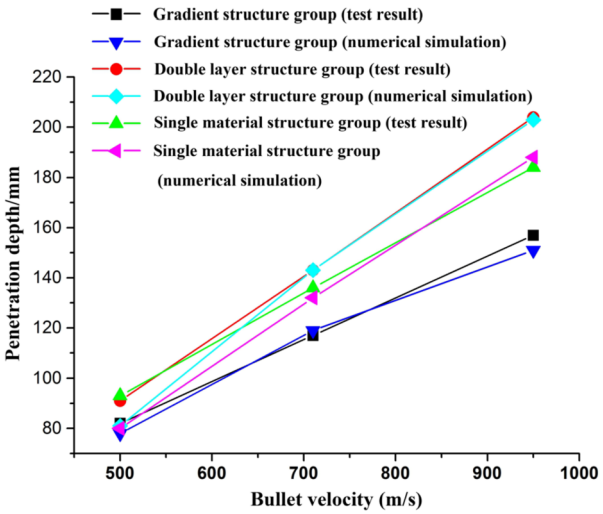


**Fig. 19** Results comparison of penetration depth of experimental and simulation

For the target of a single material structure group, because the projectile body is hindered by ultra-high performance concrete in the whole process of penetration, its penetration resistance is greater than the penetration resistance of the target of double-laminated structure group on the projectile body, so the final penetration depth is less than that of the target of double-laminated structure group.

In order to check and verify the accuracy and consistency of the numerical simulation results and the experimental results, the penetration depth of the target with gradient structure, double-laminated structure, and single material structure under three different penetration velocities of projectile bodies is compared and analyzed according to Fig. 13 and its curve fitting formula. The results are shown in Fig. 19. When the penetration velocity of the projectile body is 500 m/s, the penetration depth of the gradient structure group target obtained by experimental, theoretical calculation is not much different from that obtained by numerical simulation calculation. However, there is a difference of about 10 mm between the penetration depth calculated by the theoretical sample and that calculated by numerical simulation for both the double-laminated structure group and the single-material structure group, which may be related to the setting of projectile penetration velocity during the test. However, when the penetration velocity of the projectile body is 710 m/s and 950 m/s, the penetration depth of the target of the gradient structure group, the target of the double-laminated structure group, and the target of the single material structure group has good agreement with the penetration depth of the numerical simulation calculation. In summary, the test results agree with the numerical simulation results.

### 4.3 Failure characteristic analysis of target

Based on the research of penetration depth of projectile body under different structural materials, it is found that the excellent penetration resistance performance of the gradient structure group target is more obvious with the increase of projectile penetration velocity. Therefore, in order to further optimize the design of functionally graded structural materials and conduct a comprehensive study on their properties, the stress distribution and failure characteristics of high-impact functionally graded structural targets, dual-laminated structural

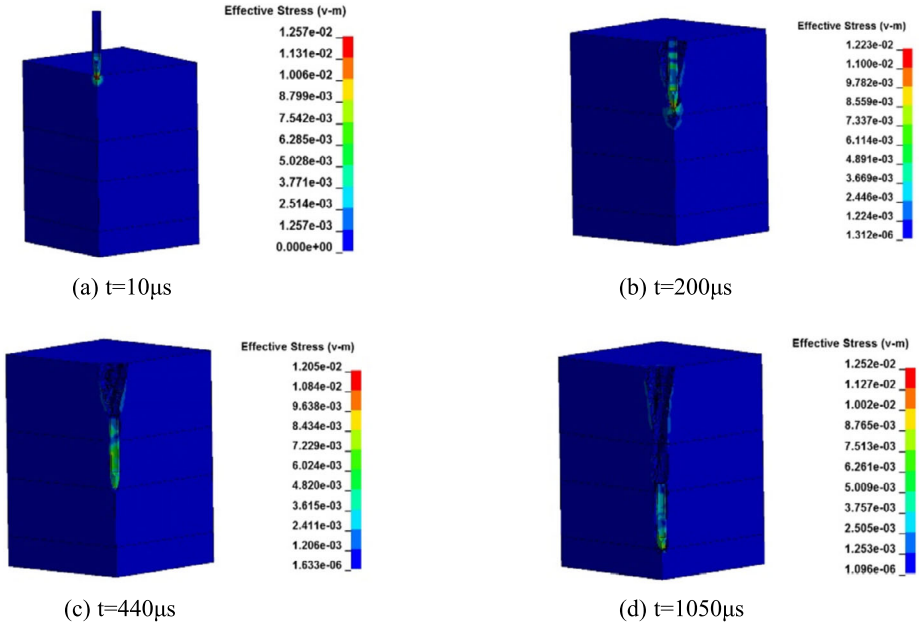


**Fig. 20** Stress cloud diagram of a gradient structure group target at different times

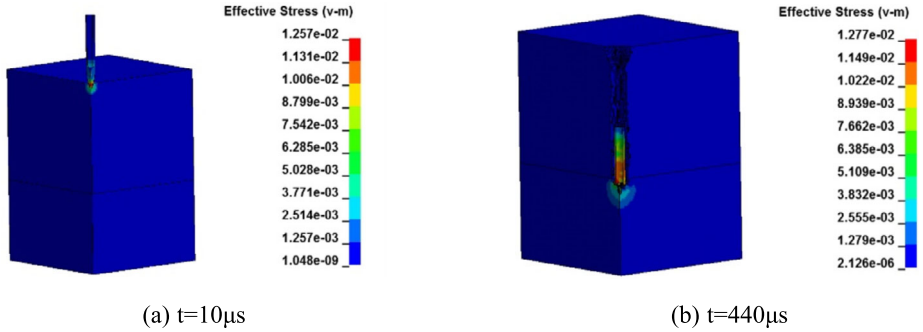


**Fig. 21** Stress cloud diagram of a double layer structure group target at different times

targets, and single-material structural targets at some time under the penetration of 950 m/s projectiles are studied based on numerical simulation (Fig. 20, Fig. 21, and Fig. 22).

The stress nephogram of the target of the gradient structure group under the action of projectile body penetration is shown in Fig. 20, from which it can be clearly seen the pitting phenomenon of the target of the gradient structure group during the process of projectile body penetration and the formation of penetration depth. Due to the relatively high velocity of the projectile body, when the projectile body collides with the target of the gradient structure group, a large impact stress will be generated at the contact surface between the projectile head and the target (Fig. 20(a)). The concrete target will suffer compression and shear failure under the strong impact stress, thus forming a funnel-shaped crater, and the projectile body will also suffer a large impact reaction force (Fig. 20(b)). With the increase of

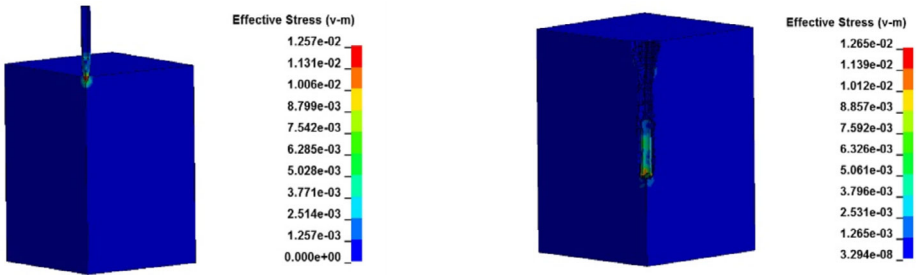


(a) t=10μs (b) t=440μs

**Fig. 22** Stress cloud diagram of a single material structure group target at different times

penetration time, the projectile will continue to penetrate the gradient structure group of targets along the funnel-shaped pit and then form columnar penetration channels (Fig. 20(c)). With the extension of penetration time, the projectile body formed a penetration channel with greater depth in the target of the gradient structure group, and the diameter of the channel is slightly larger than that of the projectile body (Fig. 20(d)).

Relative to the gradient structure group target, the first layer structure of the double-laminated structure group target is also composed of ultra-high performance concrete, while the single material structure group target is all composed of ultra-high performance concrete. Therefore, when the projectile penetration velocity is the same, the hole diameter and hole area on the positive penetration surface of the target of the double-laminated structure group and the target of the single material structure group should be similar, and the numerical size should also be similar, which can be demonstrated from Figs. 21(a) and 22(a). However, compared with the target of the gradient structure group, the second layer structure of the target of the double-laminated structure group is composed of porous ceramsite concrete, and its strength and toughness are lower than those of the target of the gradient structure group. Therefore, the resistance to the penetration process of the projectile body is smaller, and the stress on the projectile body is also smaller (Fig. 21(b). The penetration depth of the final projectile body is relatively large. However, the strength and toughness of the target in the single material structure group are much higher than that in the porous ceramite concrete, and its inhibition effect on the projectile body penetration is stronger, so the projectile body is subjected to a larger reaction force (Fig. 22(b)). As a result, the penetration depth of the target in the single material structure group is smaller than that in the double-laminated structure group but larger than that in the gradient structure group.

A comprehensive analysis of the stress states of the gradient structure group, the double-laminated structure group, and the single material structure group at some special moments in the penetration process shows that the gradient structure group has better penetration resistance.

## 5 Conclusion

Through the experimental and numerical simulation studies on the gradient structure group, double-laminated structure group, and single material structure group at different penetration rates, the following conclusions are drawn:

(1) Through experimental studies, the relationship between projectile penetration velocity and crater diameter, crater forming area and penetration depth under the action of targets of different structural materials is explored, and the linear relationship between projectile penetration velocity and crater diameter, crater forming area and penetration depth under the action of targets of gradient structure, double-laminated structure, and single material structure is established. At the same penetration velocity, the crater area, crater depth, and penetration depth of the target in the gradient structure group are the smallest compared with the target in the double-laminated structure group and the target in the single material structure group, showing excellent penetration resistance.

(2) Through the numerical simulation, the following conclusions can be drawn: compared with the target of the double-laminated structure group and the target of the single material structure group, the target of the gradient structure group has excellent penetration resistance at the same projectile penetration velocity, and with the increase of projectile penetration velocity, the excellent penetration resistance of the target of the gradient structure group is more prominent.

(3) Compared with the double-layered structure group and the single-material structure group, when the projectile velocity is 500 m/s, the penetration depth of the gradient structure group is reduced by 3.7% and 2.5%. When the projectile velocity is 710 m/s, the penetration depth of the gradient group target is reduced by 16.8% and 9.9%, respectively. When the projectile velocity is 950 m/s, the penetration depth of the gradient group target is reduced by 25.6% and 19.7%, respectively. Through comparative analysis of the penetration depth of the projectile body under experimental, theoretical calculation, and numerical simulation calculation, it is found that the experimental results and numerical simulation results have good consistency and coincidence.

(4) In the process of projectile penetration, due to the setting of the fiber layer at the target interface of the gradient structure group, as well as the existence of the second and third structural transition layer, the resistance in the process of projectile penetration can be improved to a great extent, thus reducing the energy in the process of projectile penetration to a great extent, and finally achieving a great reduction in penetration depth.

(5) Functional-graded structural materials have a size effect, and different sizes will have a certain impact on the performance, so it is necessary to carry out relevant performance research on different sizes in different application backgrounds in the future.

(6) In the numerical simulation, more analytical perspectives should be taken, and numerical analysis of full-field plastic strain and toughness (energy) will be carried out in subsequent studies.

**Acknowledgements** The study is supported by "The Doctoral Scientific Research Foundation of Shandong Technology and Business University, China. (Grant No. BS202009)." The study is supported by "the National Natural Science Foundation of China (Project Nos. 52109165)." The study is supported by "Shandong Provincial Natural Science Foundation (Project Nos. ZR2021QG002)."

**Author contributions** Junlin Lv: writing—review and editing, formal analysis, funding acquisition. Zhiliang Ren: data curation, writing—original draft, investigation, funding acquisition. Junhong Huang: conceptualization, formal analysis, funding acquisition. All authors reviewed the manuscript.

## Declarations

**Competing interests** The authors declare no competing interests.

## References

Dancygier, A.N., Yankelevsky, D.Z., Jaegermann, C.: Response of high performance concrete plates to impact of non-deforming projectiles. International Journal of Impact Engineering **34**(11), 1768–1779 (2007)

Li, Q.M., Reid, S.R., et al.: Local impact effects of hard missiles on concrete targets. International Journal of Impact Engineering **32**(1), 224–284 (2005)

Cheng, Y., Wang, M., Shi, C., et al.: Review of experimental investigation of concrete target to resist missile impact in large velocity range. J. Zhejiang Univ. Sci. A **49**(4), 616–625+637 (2015)

Pan, H., Ma, Y.: Impact resistance of steel fiber reinforced concrete and its mechanism of crack resistance and toughening. J. Build. Mater. **20**(6), 956–961 (2017)

Sovják, R., Vavřiník, T., Zatloukal, J., et al.: Resistance of slim UHPFRC targets to projectile impact using in-service bullets. Int. J. Impact Eng. **76**, 166–177 (2015)

Tai, Y.S.: Flat ended projectile penetrating ultra-high strength concrete plate target. Theor. Appl. Fract. Mech. **51**(2), 117–128 (2009)

Wang, S., Le, H.T.N., Poh, L.H., et al.: Resistance of high-performance fiber-reinforced cement composites against high-velocity projectile impact. Int. J. Impact Eng. **95**, 89–104 (2016)

Yang, S.: Research on Penetration Resistance of New Concrete Composite Protective Layer. Harbin Institute of Technology, Harbin (2009)

Wang, F., Dong, Y., Feng, S.-s.: Numerical study on penetration performance of low-velocity flat-nose projectile into two-laminated target. J. Syst. Simul. **21**(2), 367–370 (2009)

Yang, L., Zhang, J., Zhang, Q., et al.: The study for multiplayer structure anti-penetration. J. Projectiles and Guides **25**(4), 156–158 (2005)

Huan, C., Wen, B.: Development of characterization techniques for functionally gradient materials. J. Materials Guidance **24**(15), 181–185 (2010)

Zhou, N.: Research on Penetration Resistance and Failure Mechanism of an Explosive Composite Functionally Gradient Target. Nanjing University of Science and Technology, Nanjing (2014)

Quek, S.T., Lin, V.W.J., Maalej, M.: Development of functionally-graded cementitious panel against high-velocity small projectile impact. Int. J. Impact Eng. **37**(8), 928–941 (2010)

Mastali, M., Naghibdehi, M.G., et al.: Experimental assessment of functionally graded reinforced concrete (FGRC) slabs under drop weight and projectile impacts. Constr. Build. Mater. **95**, 296–311 (2015)

Gao, S., Liu, H., Jin, L., et al.: Penetration Mechanics of Concrete. China Science and Technology Press, Beijing (2012)

Kong, L.: Study on Structure and Properties of Ceramsite Mixed Aggregate Concrete. Harbin Institute of Technology, Harbin (2008)

Wang, Y.: Numerical Simulation of Elastic Resistance of Gradient Composites. Wuhan University of Technology, Wuhan (2013)

Wei, W.L., Chen, Y.Q., Ren, X.J., Wang, J.H., Wang, Z.Q., et al.: Experimental and numerical study on the influence of plastic modified concrete as attenuation layer on explosion effect. Int. J. Struct. Stab. Dyn. **22**, 2250116 (2022). https://doi.org/10.1142/S0219455422501164